Int. J. Heat Mass Transfer. Vol. 36, No. 10, pp. 2675–2684, 1993
Printed in Great Britain

0017–9310/93 $6.00 + 0.00

Impinging jet studies for turbulence model assessment—I. Flow-field experiments

D. COOPER, D. C. JACKSON, B. E. LAUNDER and G. X. LIAO
Department of Mechanical Engineering, UMIST, Manchester, U.K.

(*Received* 21 *April* 1992)

Abstract—The paper reports an extensive set of measurements of a turbulent jet impinging orthogonally onto a large plane surface. Two Reynolds numbers have been considered, 2.3×10^4 and 7×10^4, while the height of the jet discharge above the plate ranges from two to ten diameters, with particular attention focused on two and six diameters. The experiment has been designed so that it provides hydrodynamic data for conditions the same as those for which Baughn and Shimizu [*ASME J. Heat Transfer* **111**, 1096 (1989)] have recently reported Nusselt number data (at $Re = 23\,000$). In both experiments, before discharge, the air passed along a smooth pipe sufficiently long to give fully developed flow at the exit plane of the jet—a feature that is helpful in using the data for turbulence-model evaluation. Hot-wire measurements have been made with pipes of nominally one-inch (26 mm) and four inches (101.6 mm) diameter. Data are reported of the mean velocity profile in the vicinity of the plate surface and also of the three Reynolds-stress components lying in the x–r plane. Computational results reported in a companion paper [*Int. J. Heat Mass Transfer* **36**, 2685–2697 (1993)] indicate a good degree of internal consistency between the mean and turbulent field data in that models predicting the mean flow poorly (or well) also predict the turbulence data poorly (well).

1. INTRODUCTION

THE TURBULENT jet impinging orthogonally onto a plane surface produces, in the vicinity of the stagnation point, among the highest levels of Nusselt number encountered in single-phase convection. It is thus a flow configuration that is extensively used in the process industries to achieve intense heating, cooling or drying rates. The overall heat- or mass-transfer performance of jet-impingement configurations has been examined in numerous experiments, many of which have been cited by Goldstein and Franchett [1] and Jambunathan *et al.* [2].

The impinging turbulent jet is an interesting flow from another, rather different standpoint. Models of momentum and heat transport in turbulent shear flows are invariably developed by reference to flows *parallel* to walls. Such flows can be computed economically and there is a wide variety of test data available for validation. Yet since, from a purely numerical standpoint, software is nowadays available that permits flows of arbitrary configuration to be examined, there is a strong desire to devise turbulence models that are likewise applicable irrespective of the flow's orientation relative to bounding surfaces. Yet, turbulence modelling for separated and recirculating flows is by no means in a generally satisfactory state. Figure 1 shows, for example, predicted levels of Nusselt number downstream from an abrupt pipe expansion, submitted by 11 groups for an IAHR Workshop on recirculating flows and compiled by Hutton and Szczepura [3]. The vast range in the predicted heat transfer coefficient in the vicinity of the reattachment point arises, in large measure, from inappropriate assumptions in their turbulence models about turbulent transport processes in the immediate vicinity of the wall.

The turbulent impinging jet stands out as an excellent test case for validation of turbulence models for recirculating flows for, while relatively simple (as elliptic flows go), it differs in several important respects from flows parallel to walls. For example:

- in the vicinity of the axis of symmetry, turbulence energy is created by normal straining (in a parallel flow turbulence energy generation is by shear);
- the r.m.s. fluctuating velocity normal to the wall is larger than that parallel to the wall (in a parallel flow, fluctuations normal to the wall are much smaller than other components);
- the local turbulent length scales near the wall are strongly affected by the length scales of the jet turbulence (in a parallel flow, length scales are usually determined by the distance from the wall alone);
- convective transport of turbulence energy towards the stagnation point is important (in a parallel flow, convective effects are usually negligible, an approximate balance existing between generation and dissipation processes).

One should, in addition, mention that, just beyond the impingement region, the flow structure will be significantly affected by the strong curvature of the streamlines, while at greater radii, the flow turns into a radial wall jet which has a number of interesting and hard-to-predict features in its own right; for example, maximum turbulent stress levels are more than twice as high as in the corresponding plane wall jet [4].

NOMENCLATURE

D	pipe diameter	U_{CL}	centre-line velocity in pipe
E	instantaneous bridge voltage	U_m	maximum radial velocity in wall jet
H	pipe exit height above plate	$\overline{uv}$	Reynolds shear stress
q_w	wall heat flux	u'	r.m.s. radial velocity
Nu	Nusselt number, $q_w D/\kappa(T_w - T_\infty)$	V	velocity normal to plate
Re	pipe Reynolds number $U_B D/\nu$	v'	r.m.s. velocity normal to plate
r	radius from pipe centre line	y	height above plate
t	pipe thickness	$y_{1/2}$	location where $U/U_m = 0.5$.
T	temperature		
T_w	local wall temperature		
T_∞	free stream temperature	Greek symbols	
U	radial velocity	κ	thermal conductivity
U_B	bulk velocity in pipe	ν	kinematic viscosity.

While, as remarked above, the impinging jet has been the subject of numerous experimental studies, none can be said to have been designed with the needs of turbulence modelling in mind. The heat/mass transfer investigations, with scarcely an exception, have limited attention to heat or mass flow rates *at the wall itself*. Usually, moreover, the flow conditions at exit from the nozzle are undefined and hard to guess while, in all but the most recent studies, heat conduction within the test plate brings considerable uncertainty to the true Nusselt number profile close to the stagnation point. The quite separate flow-field studies have likewise, and perhaps not unreasonably, not been designed especially to meet the needs of turbulence modelling. Here, too, jet exit conditions are usually insufficiently prescribed or the jet exit is so far above the impingement plate that a numerical study would require an inconveniently large number of grid nodes to resolve the flow field with negligible numerical error. Finally, since Nusselt number data provide the most sensitive indicator of the nature of the viscous sublayer, one really wants *both* velocity and thermal data available for the same experiment—or, at least, the same experimental conditions.

The above, together with the recent experiments of Baughn and Shimizu [5], are the considerations that have shaped the research reported in this paper. Baughn and Shimizu's recent study of the radial variation of Nusselt number in the turbulent impinging jet had three features that made it particularly useful

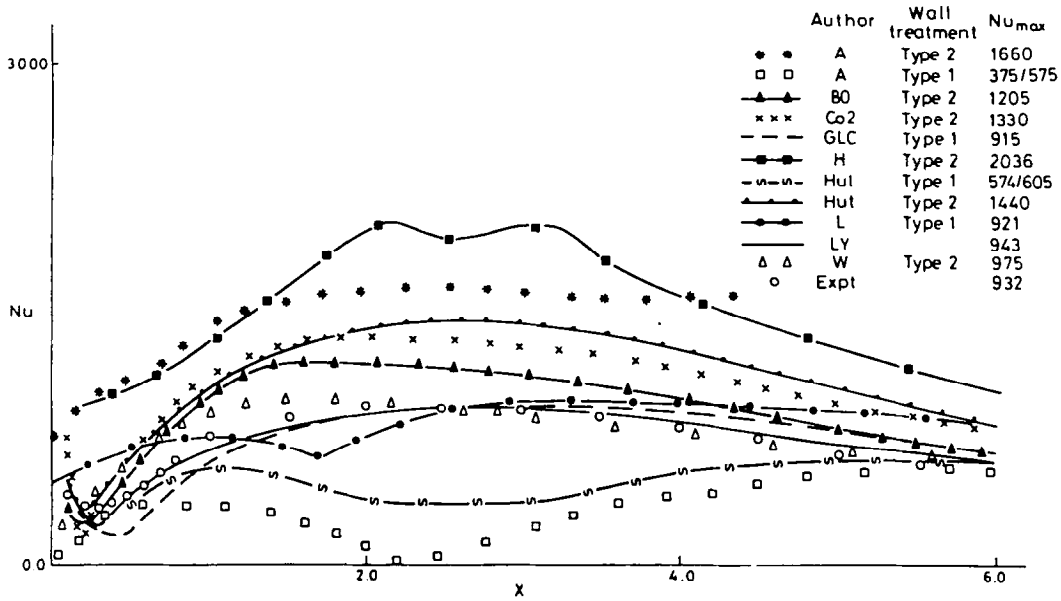

FIG. 1. Nusselt number variation downstream from an abrupt pipe enlargement ($x = 0$ marks the enlargement plane of pipe). From Hutton and Szczepura [3] and reproduced with permission.

as a bench-mark case for turbulence model assessment. First and foremost, the jet was supplied through a straight uniform-diameter pipe with a length of some 90 diameters; the flow was this assuredly fully developed at jet discharge. Secondly, the use of a vacuum deposited gold film as the heating medium essentially eliminated conduction within the test plate while, finally, experiments were taken with the jet exit as close as two diameters to the plate, thus facilitating a numerical simulation. However, in common with other thermal studies, no velocity field data were obtained. The present experiments have therefore been aimed at obtaining mean and fluctuating velocity-field data under conditions sensibly the same as those in the experiments of Baughn and Shimizu. Section 2 below details the apparatus, instrumentation and procedures while the experimental results themselves are presented and discussed in Section 3. A companion paper, Craft *et al.* [6], reports a computational study of this flow comparing the performance of a variety of turbulent transport models.

2. THE EXPERIMENTAL PROGRAMME

2.1. *Apparatus and instrumentation*

The experiments were carried out with two different pipe configurations. The first series employed a copper pipe of 1.025 in (26 mm) internal diameter, 2.1 m in length giving a length : diameter ratio of 80 : 1. Air was supplied from a centrifugal blower via flexible tubing. At the inlet to the copper tube, a flow-straightening honeycomb was fitted in the form of drinking straws glued together. The flow rate through the pipe was controlled by a bleed valve. The second series employed a 4 in. (101.6 mm) diameter brass pipe 81 diameters in length. This was preceded by a further section of slightly smaller diameter pipe (99 mm) giving a total run of 12.5 m or 125 diameters. In this case the flow entered the pipe by way of a contracting section and the air supply rate was controlled by a variable speed d.c. fan. This larger diameter rig is used in our laboratory teaching programme a dozen times a year for a detailed study of pipe flow: suffice it to say here that the measured flow properties near exit conform very well with those for fully developed pipe flow including a rigorously linear variation of shear stress across the pipe.

In both series the bulk velocity along the pipe was inferred from a measurement of the pipe centre-line velocity with a pitot tube. White [7] gives a tabulation of the connection between centre-line and bulk velocity as a function of Reynolds number to which the following relation has been fitted

$$U_B/U_{CL} = 0.811 + 0.038(\log(Re) - 4) \qquad (1)$$

Re being the usual pipe Reynolds number. The centre-line velocity was measured immediately before and immediately after each traverse of the near-plate velocity profile.

One small difference between the two apparatuses is noted. For the large diameter pipe, the outer diameter was 4.25 in. giving a pipe wall thickness (t) of 0.0313 D while for the smaller diameter the outer diameter of 1.145 in. gives $t/D = 0.112$.

The rectangular test plate on which the flow impinged, measuring 1275 × 975 mm, was made from printed-circuit board fixed to a 25 mm thick plywood backing. The copper film of the circuit board faced the impinging flow and thus enabled the probe's contact with the wall to be identified electrically. A steel frame was screwed to the back of the plywood and this, in turn, was secured to a milling machine tool bed thus allowing the plate to be moved in a plane orthogonal to the jet axis. Three probe access holes were bored in the test plate to allow (in combination with moving the plate itself) profiles to be obtained at the desired radius ratios without excessively displacing the plate centre from the stagnation point.

The probe-traversing unit was a precision-built instrument with anti-blacklash gearing and a range of 100 mm. The probe shaft was driven by a stepper motor controlled by a micro-computer with a minimum forward step of just under 2.3 μm. The smallness of this step increment made it possible to use the electrical-contact method as a means of determining accurately the probe's position with respect to the wall.

Measurements in the impinging jet were made with a TSI IFA-100 two-channel hot-wire anemometer interfaced to a data acquisition system. The output voltages from the bridge were fed into a 12-bit ADC in the acquisition system and the values stored in the computer memory. No linearizer was used as 'look-up' tables were incorporated into the computer software to convert the bridge output voltages into velocities. Standard DISA hot-wire probes were employed. For the measurements with a single normal wire initially a 55P11 probe (with its prongs bent downwards towards the test plate) was used. Later a 55P05 boundary-layer probe with a gold-plated wire was adopted. In duplicate runs made with the new probe, no material differences were noted from the earlier measurements. Cross-wire measurements were all made with a miniature probe 55P61.

2.2. *Experimental procedure*

The hot-wire probes were calibrated in a separate facility, the calibration being based on ten equi-spaced velocity increments covering the velocity range of interest. A least squares curve of the form:

$$E^2 = A + BU^{1/2} + CU$$

was fitted to the points where E is bridge voltage and U the velocity. The cross-wire probes were also calibrated in yaw. Before removing the probes from the calibration rig, validation checks were made on the agreement of the least squares fit with the individual data points. Likewise, as a further check, the yaw calibration was used to determine the angle at

which the probe was actually aligned: the maximum admissible error was $\pm 0.3°$.

In the impinging jet measurements, two velocity profile traverses were always sandwiched between probe calibrations. The 'before' and 'after' calibrations were compared and the data for the velocity profiles were retained only if the average difference in the calibrated velocities was less than 2%.

Before the test programme proper began, extensive validation checks were made to ensure the flow's symmetry. For this purpose, profile measurements were made at 90° intervals around the jet for different normalized jet heights (H/D) and radius ratios (r/D). The results of these tests indicated that the profiles at different angular positions were indistinguishable from one another.

The experimental programme has covered height: diameter ratios of 2, 3, 4, 6 and 10 though the greatest emphasis has been given to the case where $H/D = 2$: this represented both the easiest case to simulate numerically and was one for which heat transfer data [5] were available. For the 26 mm diameter pipe, measurements extended up to $r/D = 9$ and for the larger diameter pipe to $r/D = 3$, the latter limit being set partly by the lower velocities and partly to avoid 'edge' effects. Measurements in the smaller pipe were made at a nominal Reynolds number of 2.3×10^4 only, while, in the larger pipe, at Reynolds numbers of 2.3×10^4 and 7.1×10^4. However, in this larger pipe, at the lower Reynolds number, only the two smaller values of H/D were considered. There is thus a reasonable degree of overlap between the experiments in the two pipes and, as will be seen later, a satisfactory level of accord exists between the two sets.

While both single- and cross-wire measurements were taken with both pipes, only those obtained with the larger pipe are reported here due to the thinness of the wall jet in the case of the smaller pipe. For every position in the velocity traverse ten batches of 512 data points per wire were recorded, the points in each batch being gathered at 100 samples per second with a short interval between each batch. The mean and r.m.s. values of velocity and the mean cross-correlation were evaluated from these 5120 data points.

Absolute accuracies of the data are difficult to assess and, indeed, vary greatly across the flow. However, the maximum mean velocity at any position relative to the bulk velocity is believed to be accurate within $\pm 2\%$. Root-mean-square fluctuating velocities have a corresponding estimated uncertainty of $\pm 4\%$ (u') and $\pm 6\%$ (v') for values of y less than $y_{1/2}$ while turbulent shear-stress ($\overline{uv}$) uncertainties are typically of the order of $\pm 9\%$ except near the jet impingement point and other regions where the correlation coefficient $|\overline{uv}|/(u'v')$ is smaller than about 0.2. There are two other indications of the data's internal consistency: the rate of growth of the impinging jet for $H/D = 10$ corresponds closely with the asymptotic growth of the radial wall jet [4] while, as the companion paper [6] shows, turbulence models displaying best accord with the mean velocity also achieve the best agreement with the turbulence field.

Space constraints preclude a complete presentation here of all the data gathered in this study. However, those interested in obtaining a set of the test data in machine readable format should send their requests to Mr D. C. Jackson at UMIST.

3. PRESENTATION AND DISCUSSION OF RESULTS

First, to place the range of results in context, Figs. 2 and 3 show for the smaller 26 mm pipe the variation of $y_{1/2}/D$ and $(U_m/U_B)(r/D)$ as a function of radial distance from the stagnation point. Figure 2 indicates that, away from the immediate vicinity of the stagnation point, the radial wall jet grows linearly with distance but that the slope, over the region covered, increases slightly with jet discharge height. As the height of the jet above the impingement point is increased, more mixing occurs before the jet strikes the plate and (as we shall shortly note) turbulence levels are higher. This increase of spreading rate accords with the behaviour noted in the wall jet review of ref. [4]. If the normalized velocity profile was invariant with radius and the loss of momentum due to wall friction was negligible, the quantity (U_m/U_B) (r/D) would be constant. From Fig. 3 it is seen that this quantity increases rapidly with distance from the stagnation point up to a distance (depending on the discharge height) of 2–3 diameters. This we can regard as the *impingement zone* of the jet and it is on this region (values of r/D up to 3.0) that most attention has been focused in this study. At greater radii the parameter is fairly uniform, especially for the larger values of H/D where the approach to self-similar conditions is more complete.

Let us now examine in more detail the near-wall behaviour. Figures 4 and 5, again for the case of the 26 mm pipe, examine the variation of mean and fluctuating velocity on the pipe axis, $r = 0$. For the case where $H/D = 6.0$, Fig. 4 tracks the development of the flow approaching the stagnation point over the last 3.5 diameters nearest the wall. A mean fluid packet

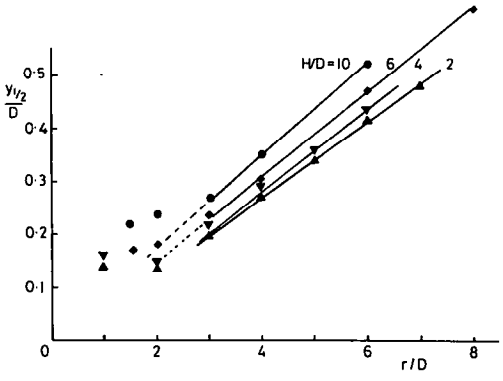

FIG. 2. Radial growth of jet half width, $y_{1/2}$.

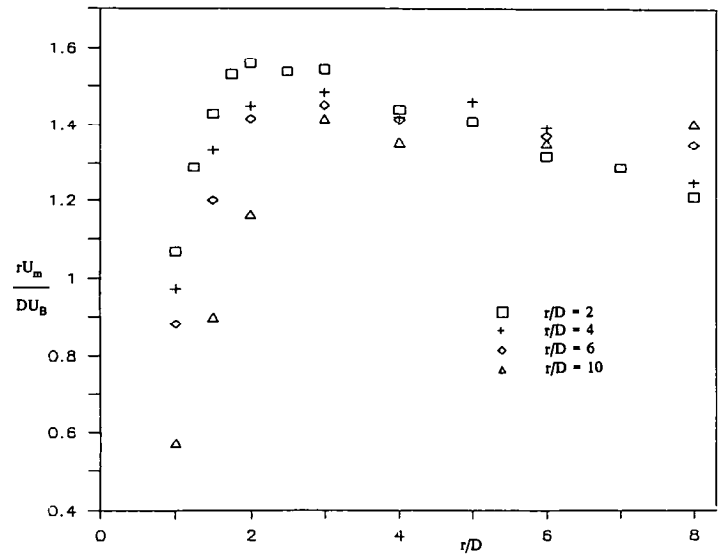

FIG. 3. Variation of $(rU_m)/(DU_B)$ with radius.

proceeds from the right (larger y/D) towards the wall. Over most of this region the mean velocity on the axis is falling slowly due mainly to the action of turbulent shear stresses;† the jet is little affected by the wall. Within about $0.7D$ of the surface, however, the wall provokes a more pronounced deceleration of the fluid. The streamwise (wall-normal) turbulence intensity increases smoothly up to a distance of about $0.3D$ from the wall, a development that is presumably due to the diffusion of turbulence from the mixing region of the jet where it is produced. Then, however, there is an abrupt *decrease* in fluctuating velocity followed by a marked increase. The decrease is believed to be due to the wall exerting a damping effect on the turbulent fluctuations normal to the wall (via the agency known as the *pressure–strain* process); the apparent abrupt rise for $y/D < 0.1$ is, we believe, mainly due to the single hot-wire becoming sensitive to fluctuations *parallel* to the wall as the mean velocity falls to zero.

The behaviour of v' on the axis in the immediate vicinity of the wall is shown in Fig. 5 for the range of

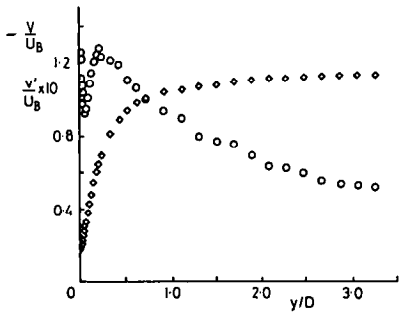

FIG. 4. Variation of axial mean and turbulent velocities along symmetry axis as jet approaches stagnation point. ◇ Mean axial velocity, ○ r.m.s. turbulent velocity.

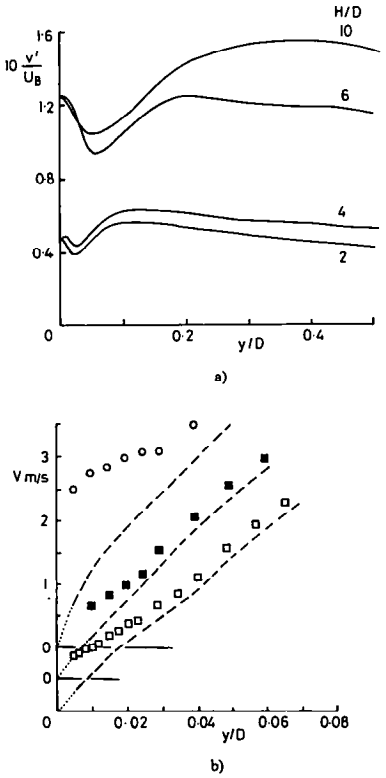

FIG. 5. Dependence of near-wall axial mean and turbulent velocities on height of pipe exit: (a) r.m.s. turbulent velocities; (b) mean velocity. □ $H/D = 2$; ■ $H/D = 4$; ○ $H/D = 6$; ---- Mean velocity corrected according to equation (2).

†Since the flow in the pipe is fully developed at discharge, there is a non-zero shear–stress gradient tending to decelerate the fluid near the axis.

jet discharge heights considered. A notable feature is that the turbulence intensity profiles for $H/D = 2.0$ and 4.0 are very similar to one another, showing only a small near-wall peak and levels of turbulence intensity barely half of those for $H/D = 6.0$ and 10.0. These differences are mainly due to the fact that, for $H/D = 4.0$ and below, the mixing layer that springs from the pipe rim will not have spread to the jet axis. The other item deserving comment is the fact that the indicated mean velocity does not vanish at the wall, the apparent slip velocity being particularly high for $H/D = 6$ and 10. This anomalous indication arises from the fact that, as the mean velocity tends to zero, the 'mean' hot wire signal is increasingly affected by turbulent velocity fluctuations. If we assume the velocity fluctuations to be isotropic, to first order the corrected mean velocity V_c may be obtained as

$$V_c = \sqrt{(V^2 - \overline{2v^2})}. \quad (2)$$

The mean velocity corrected in this way is indicated by a broken line on these figures. The correction does, indeed, significantly reduce the mean velocity very near the wall while having a negligible influence further away.†

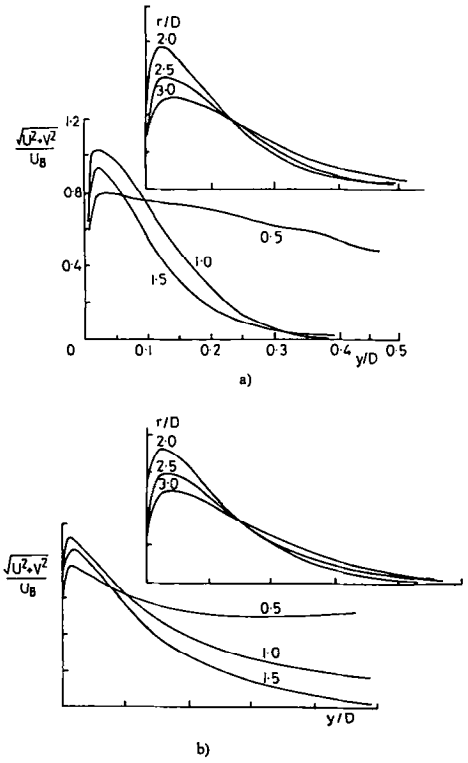

FIG. 6. Development of mean velocity with radius: (a) $H/D = 2$; (b) $H/D = 6$.

†The correction is here included for illustration only. It has not been applied to any of the other data sets. Away from the stagnation point region, mean velocities in the near-wall region are much larger in relation to the turbulent fluctuations and errors from this source of less significance.

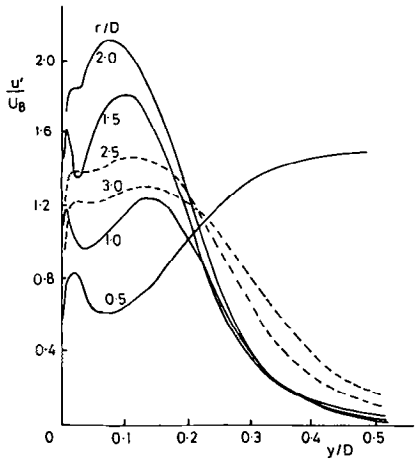

FIG. 7. Radial r.m.s. turbulent velocity profiles, $H/D = 2$, $Re = 23\,000$; 26 mm pipe.

The radial development of the single-wire mean and fluctuating velocities is shown in Figs. 6–10. The mean velocity profiles show rather small variation with jet discharge height so these are shown in Fig. 6 only for $H/D = 2.0$ and 6.0. We note that (neglecting turbulence effects) the mean velocity recorded by the hot wire is $\sqrt{(V^2 + U^2)}$. At most positions this is negligibly different from U, the mean velocity component parallel to the wall; however, at $r/D = 0.5$, the contribution of V to the signal is the dominant one away from the vicinity of the wall. Likewise, the r.m.s. turbulence intensity, u', shown in Fig. 7–10, should strictly be interpreted as that in the direction of the mean velocity vector; again, except at $r/D = 0.5$, this is very nearly that in the radial direction. Although there are quantitative differences in the radial development according to the height of the jet discharge above the plate, the qualitative behaviour is similar in all cases. The main differences in the r.m.s. profiles spring from the different levels of fluctuating velocities on the axis, already noted. For H/D of 4 and below

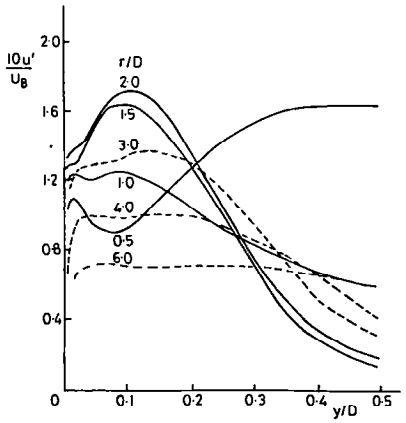

FIG. 8. Radial r.m.s. turbulent velocity profiles, $H/D = 4$, $Re = 23\,000$; 26 mm pipe.

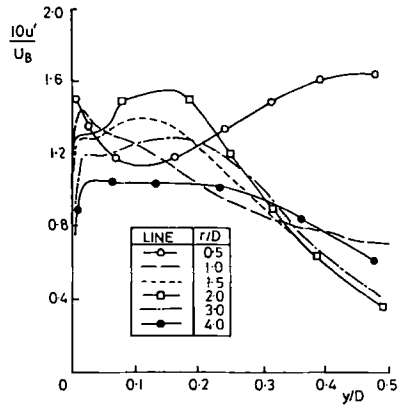

FIG. 9. Radial r.m.s. turbulent velocity profiles, $H/D = 6$, $Re = 23\,000$; 26 mm pipe.

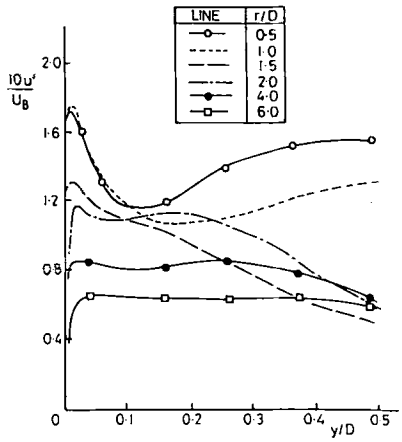

FIG. 10. Radial r.m.s. turbulent velocity profiles, $H/D = 10$, $Re = 23\,000$; 26 mm pipe.

(the profiles at $H/D = 3.0$ are very similar to those at 2.0 and are thus not included), there is initially ($r/D = 0.5$) a marked increase of u'/U_B as one moves away from the axis of symmetry both near the wall and further away. The increase near the wall (which occurs also for $H/D = 6$ and 10) arises from the shear induced by the flow's acceleration away from the stagnation point. The increase at greater distances from the wall simply reflects that the line of traverse passes through a more energetic part of the turbulent mixing layer springing from the pipe lip. At $H/D = 10$ there is no outer region increase because at this height the mixing layers have spread to the jet axis. There is a very marked reduction in turbulence intensity at $r/D = 1.0$ (except at $H/D = 10$) again to a large extent due to the fact that, at this radius, the traverse line cuts across the impinged jet. There also appears to be a secondary effect due to the stabilizing streamline curvature (the curvature is stabilizing when, as here, the angular momentum increases in the direction of increasing radius of curvature of the streamlines, Bradshaw [9]). At greater distances from the stagnation point, streamlines are nearly parallel to the surface and, significantly, the fluctuating velocities grow for a time. As the shear weakens, however, levels fall gradually with increasing radius and the turbulence intensity takes on a virtually uniform level from the edge of the sublayer to the half width of the wall jet.

It is instructive to compare the near-wall turbulence intensities with the radial variation of Nusselt number measured by Baughn and Shimizu [5], Fig. 11. Firstly, at the stagnation point, there is a 10% increase in Nu as H/D is raised from 2.0 to 6.0; as noted in Fig. 5,

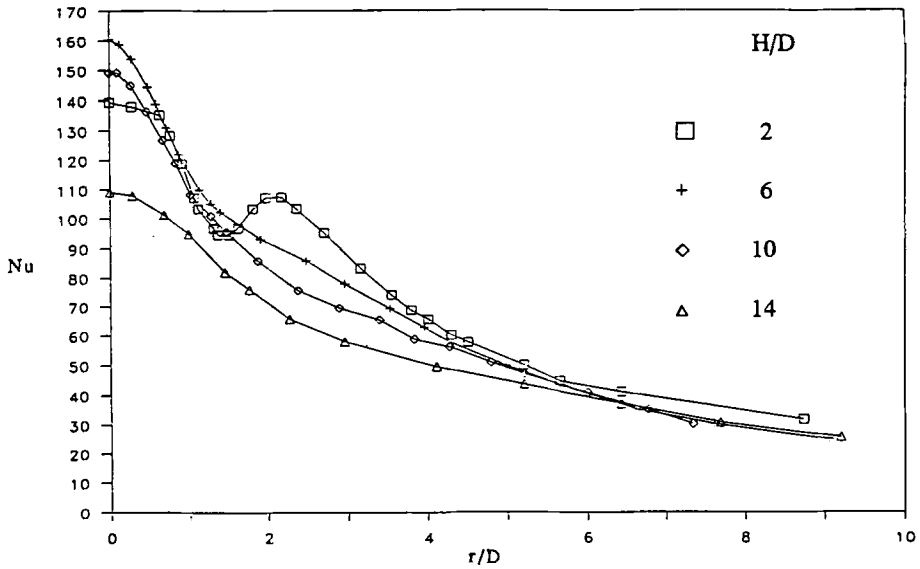

FIG. 11. Heat transfer along the plate for an ambient temperature jet for different nozzle-to-plate heights, Baughn and Shimizu [5], reproduced by permission.

increasing the discharge height of the jet also brings about a corresponding increase of turbulence intensity from 4.5 to 12.5%. It might be observed that the augmentation of Nu is not great in view of the far higher turbulence intensities. One should note, however, that the thermal boundary layer at the stagnation point is effectively confined within the viscous sublayer, so turbulence levels there have only a secondary effect on Nusselt number. As noted above, at $H/D = 2.0$ wall-adjacent turbulence levels rise from 4.5% at the stagnation point to a maximum of about 18% at $r/D = 2.0$; there is, in particular, a marked increase between $r/D = 1.5$ and 2.0. By contrast, the intensities for $H/D = 6$ and 10 are about the same at $r/D = 2.0$ as at the stagnation point while between $r/D = 1.5$ and 2.0 the levels are uniform for $H/D = 6.0$ and decrease for $H/D = 10$. We note that over the same interval ($1.5 < r/D < 2.0$) Baughn and Shimizu find that the Nusselt number increases for $H/D = 2.0$, while it decreases slightly for $H/D = 6.0$ and more steeply for $H/D = 10$. There is thus seen to be a direct link between the near-wall level of turbulence and the Nusselt number. While this is not a surprising connection, it nevertheless is one that needs to be made.

Further examination of the flow will focus on the impingement region ($r/D \leqslant 3$) and principally on the data obtained with the larger diameter pipe. The profiles at the same Reynolds number for the one-inch and four-inch pipes are in reasonably close accord except that in the outer region the profile arising from the smaller pipe is somewhat more diffuse, probably due to the relatively thick lip in the case of the 1-inch pipe, Fig. 12.

At $H/D = 2.0$ and 3.0, measurements in the four-inch diameter pipe have been obtained at two Reynolds numbers differing by a factor of three. The two H/D's show the same interesting effects of Reynolds number so here we report data only for $H/D = 3.0$. Profiles of u' and U are shown for two radial positions

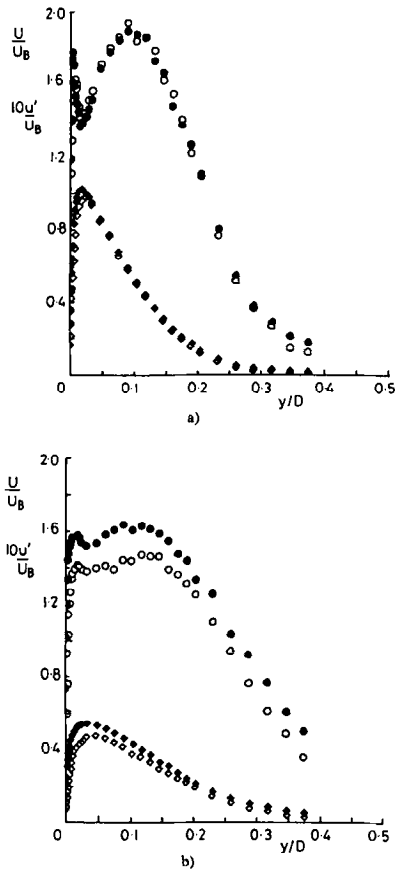

FIG. 13. Effects of Reynolds number, $H/D = 3$. Open symbols $Re = 23\,000$; filled symbols $Re = 70\,000$. ◇—Mean velocity; ○—r.m.s. turbulent velocity: (a) $r/D = 1.5$; (b) $r/D = 3.0$.

in Fig. 13. At a given radius the normalized peak mean velocity is higher by 5–12% at the larger Re and the maximum occurs closer to the wall. The latter is a known effect of Reynolds number on the shape of the velocity profile in a wall jet. The turbulence intensity profiles at $r/D = 1.5$ are for practical purposes identical—at least beyond the wall sublayer. This indicates

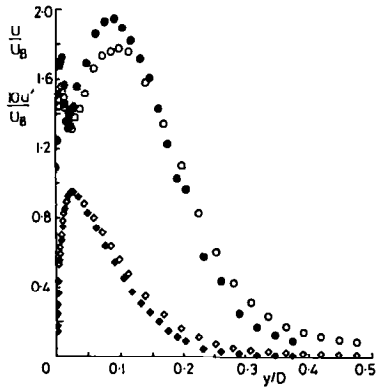

FIG. 12. Comparison of radial mean and r.m.s. velocity profiles for 1-inch and 4-inch pipes. $H/D = 2.0$; $r/D = 1.5$; $Re = 23\,000$. r.m.s. velocities: ○—1-inch; ●—4-inch. Mean velocities: ◇—1-inch; ◆—4-inch.

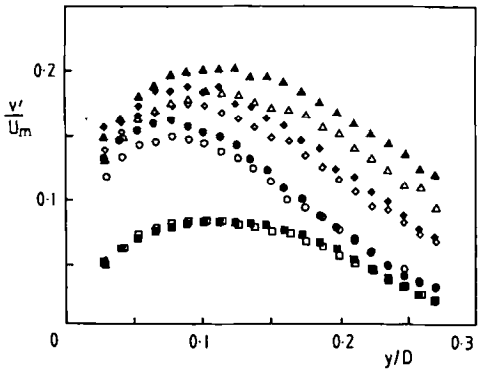

FIG. 14. Normalized r.m.s. turbulent normal velocities, $H/D = 2.0$. Open symbols $Re = 23\,000$; filled symbols $Re = 70\,000$. r/D: □—1; ○—2; ◇—2.5; △—3.0.

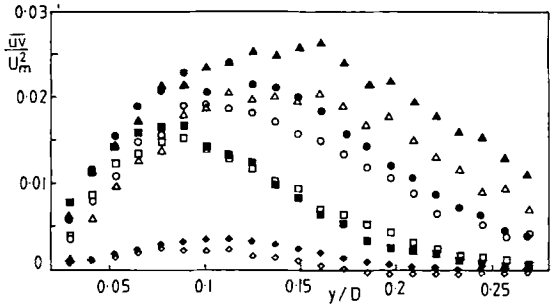

FIG. 15. Normalized turbulent shear stress, $H/D = 2.0$. Open symbols $Re = 23\,000$; filled symbols $Re = 70\,000$. r/D: ◇—1.0; □—2.0; ○—2.5; △—3.0.

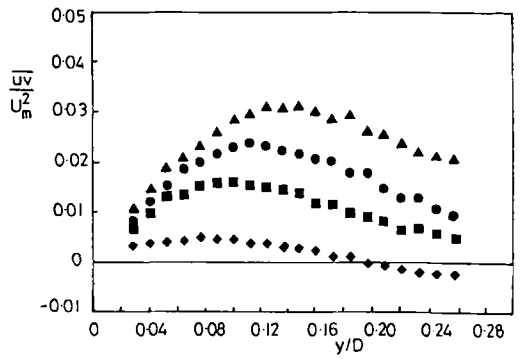

FIG. 17. Normalized turbulent shear stress profiles, $H/D = 6.0$, $Re = 70\,000$. r/D: ◆—1.0; ■—2.0; ●—2.5; ▲—3.0.

that viscosity has had no time to exert any influence on the turbulence structure. By $r/D = 3.0$, however, the sustained steeper gradients of mean velocity at the higher Reynolds number (associated with the larger value of U_m) has created a level of fluctuating velocity that is some 12% higher. Had the turbulence intensity been normalized by the local maximum rather than the bulk velocity in the discharge pipe, the apparent Reynolds number effect at this station would have disappeared (except for $y > 0.3D$ where mean velocities are so low that calibration uncertainties are relatively large).

Cross-wire measurements for $H/D = 2.0$ and 6.0 are reported in Figs. 14–18. Now the values of U and u' emerging from these measurements were typically 7–8% higher than obtained with the single wire. For this reason the v' and $\overline{uv}$ profiles reported in these figures are all normalized by the local maximum velocity measured or extrapolated from the cross wire data. In Fig. 14 the fluctuating velocities normal to the wall for $H/D = 2.0$ show peak levels that are only about 60% as high as those in the streamwise direction, a difference that is typical of that found in wall bounded thin shear flows. As with the streamwise fluctuations, in absolute terms the maximum level of v' is recorded at $r/D = 2$. When normalized by the wall jet maximum velocity, however, the intensity levels rise progressively downstream. The profiles at the two Reynolds numbers display nearly the same shapes and magnitudes though the levels are a little higher at $Re = 70\,000$. The corresponding profiles of the turbulent shear stress appear in Fig. 15. Again, the largest recorded shear stress appears at $r/D = 2.0$ whereas the profiles of $\overline{uv}$ normalized by U_m^2 also rises steadily with downstream distance. While the profiles at the two Reynolds numbers are virtually identical at $r/D = 2.0$, further downstream the normalized shear stresses at $Re = 23\,000$ become progressively lower

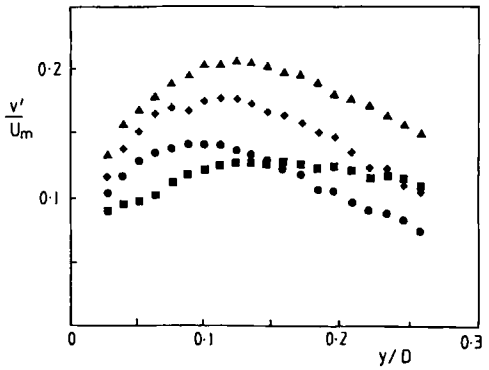

FIG. 16. Normalized r.m.s. turbulent normal velocities, $H/D = 6.0$, $Re = 70\,000$. r/D: ■—1.0; ●—2.0; ◆—2.5; ▲—3.0.

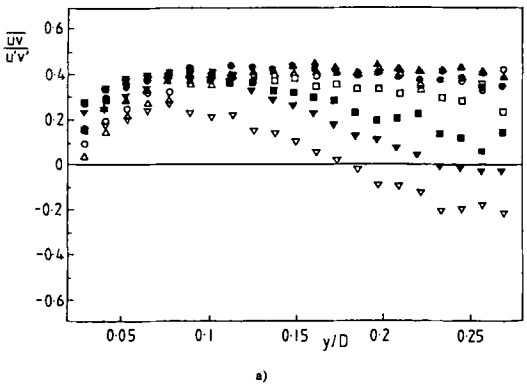

FIG. 18. Development of correlation coefficient in radial wall jet. (a) $H/D = 2.0$; Open symbols $Re = 23\,000$; filled symbols $Re = 70\,000$. r/D: ▽—1.0; □—2.0; ○—2.5; △—3.0. (b) $H/D = 6.0$; $Re = 70\,000$. r/D: ◆—1.0; ■—2.0; ●—2.5; ▲—3.0.

than those at 70 000. The relatively large errors associated with the use of cross wires at low Reynolds numbers are well known (see, for example, Tutu and Chevray [10]) and it appears likely that for v' and $\overline{uv}$ the data at the higher Reynolds number are the more accurate.

The corresponding data of turbulence intensity normal to the wall and the shear stress for $H/D = 6.0$, $Re = 70\,000$ are shown in Figs. 16 and 17. The variation of both quantities with radial position is rather less than at $H/D = 2.0$, again in line with the u' data. Finally, it is of interest to note the variation of the correlation coefficient $\overline{uv}/u'v'$ shown in Fig. 18. We see that for both $H/D = 2.0$ and 6.0, as the wall jet develops downstream, the correlation coefficient, which is initially negative in the outer region due to the curvature of the streamlines at $r/D = 1.0$, rises steadily to a nearly uniform plateau level. For $H/D = 2.0$ the plateau level is about 0.43 which is similar to values reported in many other parallel thin shear flows. The asymptotic level for $H/D = 6.0$ is reached earlier and the magnitude of the correlation coefficient is a little higher.

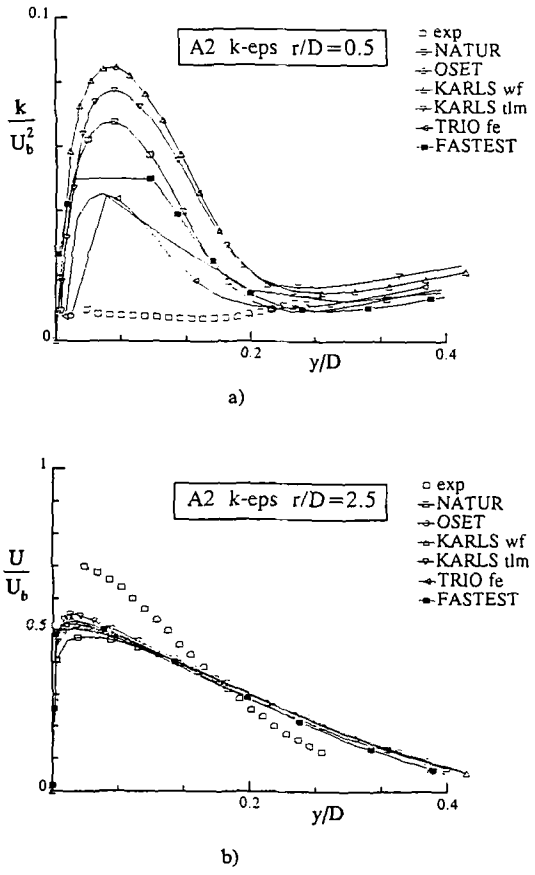

FIG. 19. Comparison of predictions of impinging jet with experiment. $Re = 23\,000$; $H/D = 2.0$. Lines: computations; open square symbols: experiments (from Brison and Brun [11]—published with permission): (a) turbulent kinetic energy profiles at $r/D = 0.5$; (b) radial mean velocities at $r/D = 2.5$.

4. CLOSING REMARKS

The experiments reported in the preceding section were carried out to provide data suitable for assessing the adequacy of engineering turbulence models at predicting impinging and related shear flows. A companion paper [6] will confirm that the group of flows under study does indeed serve as a powerful discriminator between models. As a prelude to that, Fig. 19 provides an extract from the 14th IAHR Workshop on Refined Flow Modelling organized at Lyon in October 1991 by Brison and Brun [11]. This workshop adopted as its test case the data discussed in the preceding section at $Re = 23\,000$ and $H/D = 2.0$. The figure indicates that the level of turbulence energy (k) near the stagnation point computed by half a dozen contributors using k–ε eddy viscosity models is an order of magnitude higher than measured. It is this excessive turbulence energy that leads to much too high entrainment rates of free-stream fluid. Consequently, by $r/D = 2.5$ (Fig. 19(b)) the computed wall-jet is too thick and the level of peak velocity considerably too low.

Acknowledgements—Mr G. X. Liao's contribution was made during his stay at UMIST under the Academic Links with China Scheme (ALCS), organized and sponsored by the British Council. Thanks are due to Dr L. J. W. Graham for a helpful discussion of the results. Mrs J. Buckley skilfully word-processed the manuscript for publication.

REFERENCES

1. R. J. Goldstein and M. E. Franchett, Heat transfer from a flat surface to an oblique impinging jet, *ASME J. Heat Transfer* **110**, 84–90 (1988).
2. K. Jambunathan, E. Lai, M. A. Moss and B. L. Button, A review of heat transfer data for single circular jet impingement, *Int. J. Heat Fluid Flow* **13**, 106–115 (1992).
3. A. Hutton and R. T. Szczepura, Turbulent flow and heat transfer in a sudden pipe expansion: a comparison of current models of turbulence, CEGB Rep. TPRD/B/0926/R87 (1987).
4. B. E. Launder and W. Rodi, The turbulent wall jet—measurement and modelling, *Ann. Rev. Fluid Mech.* **15**, 429 (1983).
5. J. W. B. Baughn and S. Shimizu, Heat transfer measurements from a surface with uniform heat flux and an impinging jet, *ASME J. Heat Transfer* **111**, 1096 (1989).
6. T. J. Craft, L. W. G. Graham and B. E. Launder, Impinging jet studies for turbulence model assessment—II. A comparison of the performance of four turbulence models, *Int. J. Heat Mass Transfer* **36**, 2685–2697 (1993).
7. F. M. White, *Fluid Mechanics* (2nd Edn), p. 310. McGraw-Hill, New York (1986).
8. A. Tailland and J. Mathieu, Jet pariétal, *J. de Mécanique* **6**, 103 (1967).
9. P. Bradshaw, effects of streamline curvature on turbulent flow, *AGARDograph* **16** (1973).
10. N. K. Tutu and R. Chevray, Cross-wire anemometry in high-intensity flows, *J. Fluid Mech.* **71**, 785 (1975).
11. J. F. Brison and G. Brun, Round normally impinging turbulent jets, 15th Meeting of IAHR Working Group on Refined Flow Modelling, ECL, Lyon (1991).